STARS

The Pegasus Review: UCF Undergraduate Research Journal

Volume 15 | Issue 1 Article 2

February 2022

Characterizing Particle Bed Stratigraphy as a Function of Particle Size in an Airless, Microgravity Environment

Gillian Gomer
University of Central Florida, ggomer@knights.ucf.edu

Michael Fraser
University of Central Florida, blackscape@knights.ucf.edu

Anthony Meola
University of Central Florida, tonymeola@knights.ucf.edu

Raquel Guzman
University of Central Florida, rg11145@Knights.ucf.edu

Characterizing Particle Bed Stratigraphy as a Function of Particle Size in an Airless, Microgravity Environment

Cover Page Footnote

The authors would like to acknowledge support from NASA Award #80NSSC21K0811 and #80NSSC19M0214.

Vol. 15.1 : 21-31

URJ

THE PEGASUS REVIEW:
UNIVERSITY OF CENTRAL FLORIDA
UNDERGRADUATE RESEARCH JOURNAL

Published
February 24th 2023

Characterizing Particle Bed Stratigraphy as a Function of Particle Size in an Airless, Microgravity Environment

By: Gillian Gomer, Michael Fraser, Anthony Meola, Raquel Guzman
Faculty Mentor: Dr. Adrienne Dove
UCF Department of Physics

ABSTRACT: Asteroids and other small planetary bodies are covered in a loose, dynamic layer of multi-sized dusty particles. We are focused on developing methods to further understand this surface regolith behavior to inform future landing missions on these small bodies for resource collection. The Strata-1 experiment was designed to study granular behavior in a passive, microgravity, airless environment. These conditions, simulating that of an asteroid's surface, were attained by installing Strata-1 aboard the International Space Station for 347 days. In this experiment, we took images of red, green, and blue multi-sized glass shards within a tube to better understand their stratigraphy. Images of this experiment were analyzed using a procedure written in Python to assess surface area coverage for each shard color. This paper focuses on the development of these analysis methods, which use a combination of automated and manual analysis to demonstrate the validity of methods used, as well as to characterize the particle behavior beyond position by including movement patterns amongst the colored shard groups and sub-regions of the experiment tube. Our methods proved to yield valuable insights on the shard stratification across a long duration of time. Our automated procedure offers a viable approach to future experiments which seek to understand small particle behavior in asteroidal conditions.

KEYWORDS: microgravity, regolith, stratification, image-processing, International Space Station

THE PEGASUS REVIEW:
UNIVERSITY OF CENTRAL FLORIDA
UNDERGRADUATE RESEARCH JOURNAL

URJ

Vol. 15.1 : 21-31

INTRODUCTION

Background

Instead of relying on a finite supply of resources from Earth, effective long-duration deep space exploration missions will require resources from asteroids, which must then be accessible for in-situ resource utilization (ISRU) techniques (NASA, 2012) to take advantage of on-site resources such as minerals, rare metals, and especially water. Designing equipment to collect these materials can be difficult, as asteroids and other small bodies in our solar system are typically not solid but rather are loosely aggregated with porosities of 30% to 80% (Fries et al., 2016). Even managing a successful landing on these asteroids in microgravity is complicated by rebounding and difficulties anchoring into the loose surface material (Zhao et al., 2019).

As a result of gravity, and the vibrations caused by disturbances like micrometeorite impacts, thermal cycling, and tidal effects, the granular material in asteroids will migrate, potentially creating size-segregation of particles. This stratification of particles by size is similar to the Brazil Nut Effect (BNE), where larger nuts rise and smaller nuts sink as a mixture of nuts that vary in size are subjected to vibrations (Rosato et al., 1987). It is expected that this will result in fine particles migrating below the surface to expose larger particles (Miyamoto et al., 2007), which could help explain the rough surfaces of asteroids such as Bennu and Ryugu (Chujo et al., 2018). Numerous numerical studies have been done to predict these interactions on low-gravity bodies (e.g., Matsumura et al., 2014; Maurel et al., 2017; Chujo et al., 2018). An experimental study found a roughly linear relationship between gravity levels and the rate at which large particles rise in a smaller medium due to the BNE in reduced gravity and normal air pressure, but it remained unclear if that relationship continued at microgravity levels (Güttier et al., 2013). While these studies offer useful insights into granular behavior, it remains difficult to fully simulate the volatile, low-gravity, vacuum conditions of asteroid surfaces.

To better understand these surfaces and to be able to accurately model particle interactions, the Strata-1 experiment was developed and flown aboard the International Space Station (ISS), which provides a long-term free-fall environment. Strata-1 was a passive experiment that utilized the microgravity vibrational environment aboard the ISS to study the movement, behavior, and stratification of regolith in an environment like that found on asteroids and small bodies (Dove et al., 2018). Data from the Strata-1 experiment will inform our basic understanding of these processes, as well as future space missions that include regolith sampling, landing, anchoring, and ISRU processes (Fries et al., 2018).

EXPERIMENT DESCRIPTION

Strata-1 was a NASA payload led by the Astromaterials Research and Exploration Sciences (ARES) group at NASA Johnson Space Center (JSC) with a diverse science team from institutions around the country. The experiment hardware was built and tested by the University of Central Florida (UCF), and the electronics and controls were primarily developed by the T-STAR group at Texas Tech University. After being installed on the ISS, the experiment was run from April 28th, 2016, to April 10th, 2017 (347 days), after which Strata-1 was returned to JSC for additional experiments and analysis.

The experiment hardware included four polycarbonate tubes with control electronics, lighting, and cameras to image one face of each experiment tube. Inside each tube was simulated regolith material ("simulant"), including either an ordinary chondrite meteorite simulant (UCF/Deep Space Industries CI-2), a broken-up carbonaceous chondrite meteorite containing fine and coarse particles, silicate glass shards, or spherical glass beads (Fries et al., 2018). The simulant and meteorite materials were sieved to specific size distributions, and the angular glass shards and spherical beads were composed of 2-, 5-, and 10-mm diameter particles. The glass materials were chosen to be different colors for each size to aid in image processing and analysis: red, blue, and green glass marbles were smashed in shards and sieved into 2-, 5-, and 10-mm sizes, respectively. Materials were initially loaded into the tubes in 4 layers by distinct size, with the smallest materials at either end and mid-size and large material layers in between (Fries et al., 2018), then compacted by a plate attached to an extended scissor-jack prior to and during launch and ISS delivery. After the experiment was installed on the ISS, the simulant layers were then decompressed by retracting the scissor-jack and allowed to mix. We note that initial images indicate that mixing did occur prior to the official start of the experiment, such that the materials were relatively randomly sorted but did not affect this analysis.

THE PEGASUS REVIEW:
UNIVERSITY OF CENTRAL FLORIDA
UNDERGRADUATE RESEARCH JOURNAL

URJ

Vol. 15.1 : 21-31

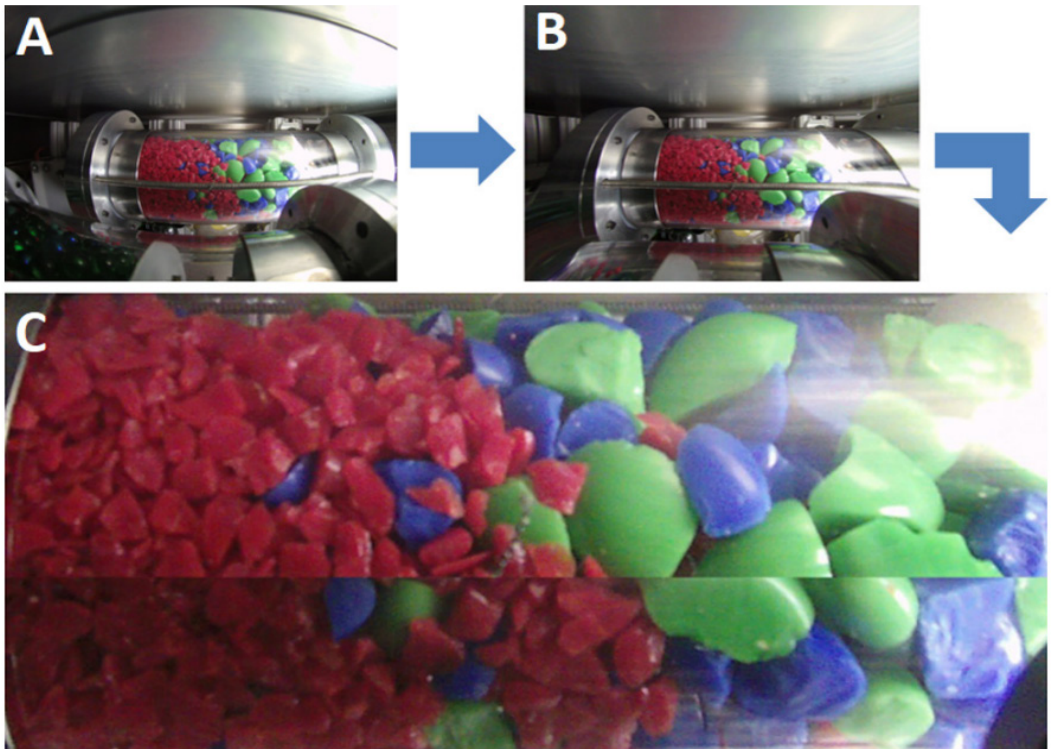

Figure 1. A.) Original image with fish-eye lens effect; B.) Manipulated image with removed distortion; C.) Final cropped image to maximize experiment view with a splice joint as a result of the metal bar removal.

Due to the size constraints of the experiment chamber, a camera that records independent red, green, and blue color channels (RGB) with a fish-eye lens was used to capture the entire length of the polycarbonate tube. Lighting was coordinated with imaging, with images captured once every 4 seconds for about 2 minutes, then in a sequence of once every 1, 2, 4, 8, 16, 32 minutes, and every 64 minutes for 960 minutes for a total sequence length of 1,024 minutes. After the completion of a 1,024 minute cycle, the imaging sequence restarted and continued with this cycle for the duration of the experiment. This sequence was chosen to avoid synchronization of images with ISS crew activity or other expected regular vibrations (Fries et al., 2018). Each tube was monitored by its dedicated camera through these series of images, which were stored on SD memory cards and then downloaded by the ISS astronaut crew.

For the purposes of the analysis presented here, we solely focus on the tube containing glass shards, hereafter referred to as Slot 1, to take advantage of the RGB image data and offer a preliminary step in analyzing all four tubes. In the following sections, we discuss our automated processing methods which were used to identify bulk particle locations within the tube, comparisons with manual analysis for a subset of the data, patterns observed over the year-long experiment, and useful insights gained from the results on particle stratification and movement behavior in microgravity.

METHODS

Pre-Processing

Over the duration of the experiment, 12,938 images of the glass shards in Slot 1 were produced. From that original dataset, 1,358 images were removed due to lighting issues (e.g., the lights not being on when the camera was taking an image) and camera malfunctions. It was then necessary to correct the fish-eye effect from the lens in order to achieve an image that closely resembled the geometry of the actual tube. To do this, we used GIMP 2.11 to remove the distortion introduced by the wide-angle lens. The straight metal bar in front of the tube, shown in Figure 1, was used as a known reference for the distortions, and we visually

1 GNU Image Manipulation Program (GIMP) is a freely distributed software for image editing. https://www.gimp.org/

THE PEGASUS REVIEW:
UNIVERSITY OF CENTRAL FLORIDA
UNDERGRADUATE RESEARCH JOURNAL

URJ

Vol. 15.1 : 21-31

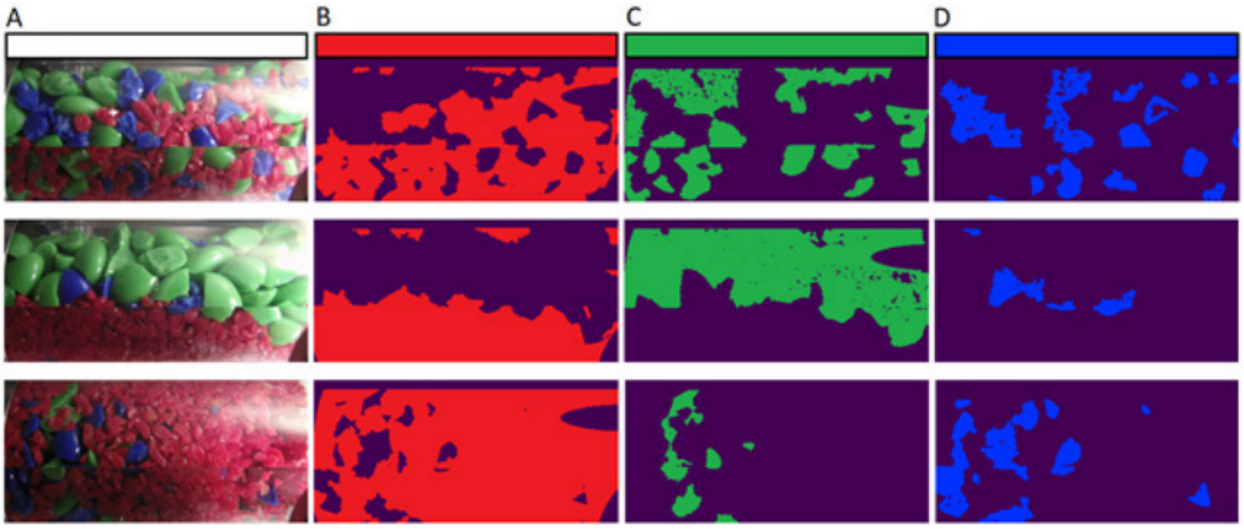

Figure 2. A.) Three examples of processed, full-color images with varying distributions of colored shards; B.) Identified red pixels from starting images with masking applied; C.) Identified green pixels from starting images with masking applied; D.) Identified blue pixels from starting images with masking applied.

determined that the fish-eye effect was removed when the bar was straight once again. Using settings within GIMP, all images were subjected to a second-order distortion of –81.613 and a fourth-order distortion of -5.291.

Following the removal of the fish-eye effect, we cropped the images to include only the relevant parts of the experiment tube. To maximize the visibility of the tube's contents, part of the metal end cap was left in view on the left edge and a different experiment tube's hardware remained visible, obscuring the view in the lower right corner. These remaining hardware pieces were later pixel-masked. To remove the static metal bar that ran the length of the tube, we used the Python Imaging Library to perform two crops of the portions above and below the bar, then spliced them back together to yield a final, pre-processed image with the maximized view of the experiment shard volume, shown in Figure 1.

To prepare for manual analysis, we isolated four subsets of images that had been pre-processed as described above, ranging from 50-200 images each. These subsets were identified close to the experiment starting time by visually noting either a large amount of shard movement activity ('Events') or very little movement across the duration of the subset before or after the Event ('Non-Events'). Non-Event 1 directly preceded Event 1 in real-time, which was followed immediately by Non-Event 2, and Event 2 occurred three days later. The results from the manual analysis of these subsets were used for both direct comparison to automated analysis results, as well as to supplement the automated data with visual insights into particle movement behavior.

Automated Analysis

We separated each pre-processed image into its independent channels for further processing, as seen in Figure 2. Within each channel, we identified pixels with 'true' values, indicating their color classification matched the color of the channel. By checking the color value of each pixel and assigning it to the channel it most closely matched, we removed duplicate identifications across multiple channels; the initial sum of identified pixels was recorded for each color. Because excess glare and shadow caused some pixels to remain uncategorized in color, we dilated the initial RGB classified pixels using the Python library Mahotas (Coelho, 2013), which expanded the identification kernel from one pixel to include the surrounding 8 pixels (9 pixels total). We then masked all pixels in visible hardware regions, areas of extreme glare, and consistently empty portions of the tube in the final pre-processed image by changing the color value of those associated pixels to 0, or black, on all channels so that it would not be identified in any channel. From the total pixel count of the image, we

THE PEGASUS REVIEW:
UNIVERSITY OF CENTRAL FLORIDA
UNDERGRADUATE RESEARCH JOURNAL

URJ

Vol. 15.1 : 21-31

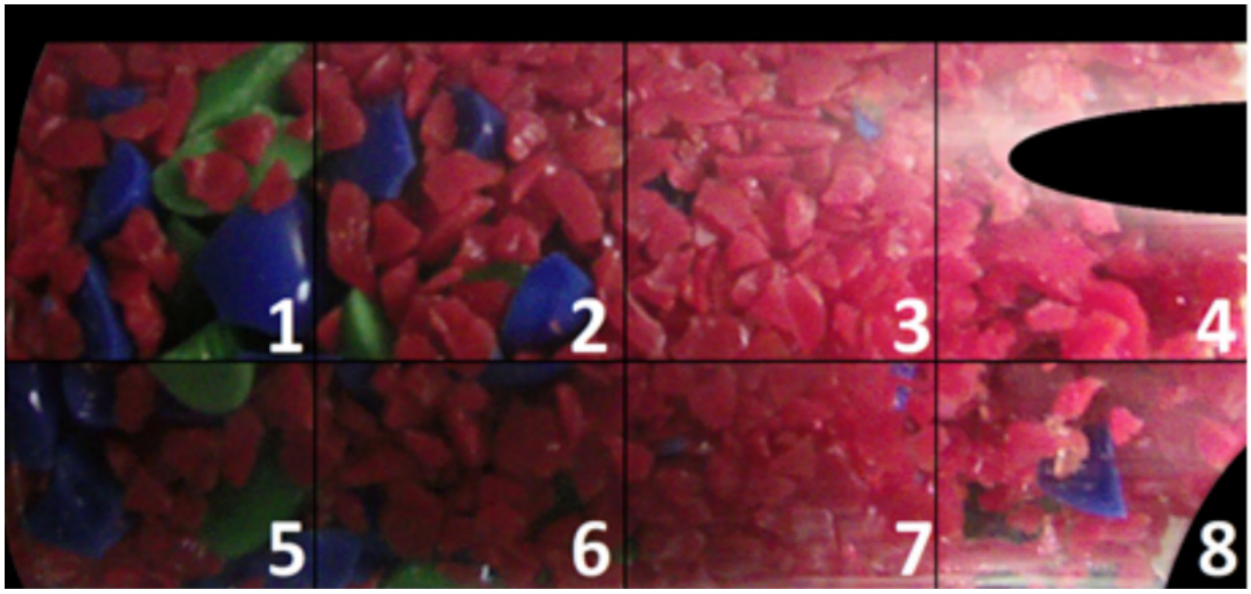

Figure 3. Fully processed experiment image with masking applied. Binned regions (1-8) used for further characterization of particle movements are shown here.

subtracted the masked pixels (11.01% of total pixels) to yield the final image to be used in data analysis. Final images measured 1459x673 pixels, containing 87,3751 unmasked pixels.

Because they were the largest percentage of material in the tube by number, we treated red shards as the background medium and sought to identify locations of blue and green shards. Each collection of touching green or blue pixels was labeled as green or blue shards, respectively. To control for regions of an identified color that were too small to likely be an actual shard (of which the smallest was roughly 750 pixels), and therefore likely identified in error, we filtered out all regions containing less than 750 pixels of a single color to result in a final identification and colored pixel count. This threshold filtered out tiny shard fragments of much smaller sizes than their parent shards, as well as miscolored regions on large shards experiencing intense glare or shadow. For analysis of particle motion, since we were unable to distinguish between individual shards due to the limited two-dimensional view and image quality, we instead sought to identify the regions where green and blue pixels were located and then look for trends in motion. After organizing each color channel image into 8 bins, shown in Figure 3 (see Appendix), the number of green and blue pixels were identified within each bin.

Manual Analysis

In addition to automated bulk analysis of the particle motion, we conducted manual tracking of particles to qualitatively characterize the behavior. We analyzed the cropped, distortion-corrected images to characterize shard locations and movements over time. Treating red shards as the background signal in the tube, we counted the number of green and blue shards visible for Non-Event 1, Event 1, Non-Event 2, and Event 2. To determine the location of specific shards over time, we used the region of interest (ROI) tool in Spotlight-162, which produced a record of the coordinates, image intensities, and other desired variables for an area identified by the user. We drew ROI boxes around each shard of a selected color to obtain a set of estimated center coordinates per image and then compiled these to look at the motion of many blue or green particles over the image sequences.

Due to the camera's variable image capturing intervals, we separated the four Events and Non-Events into further "Slow" and "Fast" subsets. "Slow" subsets were marked by 64-minute image intervals, and "Fast" subsets ranged from seconds to 32-minute intervals. We characterized the shard movement behavior by

2 Spotlight-16 is an image analysis software developed by NASA, https://ntrs.nasa.gov/api/citations/20060011194/downloads/20060011194.pdf

THE PEGASUS REVIEW:
UNIVERSITY OF CENTRAL FLORIDA
UNDERGRADUATE RESEARCH JOURNAL

URJ

Vol. 15.1 : 21-31

observing the subsets of images in rapid succession (as in a flipbook) to identify obvious movement patterns with associated movement direction, magnitude, and speed. Shard behaviors are categorized as: Translation, Swirling, Emerging, Burying, Compacting, Clustering, Dispersing, and Wiggling. Translating shards were defined as movements along the y-axis (along the long axis of the tube), whereas Emerging and Burying shards are defined by positive and negative movements, respectively, along the x-axis (either toward or away from the camera). Swirling designates shards that rotated about an axis. Clustering and Dispersing shards are characterized by the movement of shards towards or away from each other within a region, respectively, while Compacting indicates shards that became closely packed together. Wiggling shards displayed slight side-to-side or rotating movement while remaining in the same place. Additionally, we qualitatively noted the relative amount of surface area coverage for each colored shard set per image within Non-Event 1, Event 1, Non-Event 2, and Event 2.

RESULTS

For the 11,580 images processed, the total shard pixel coverage by all colors ranged from 87.20% to 111.57%, with only two images totaling 100% surface area coverage. Percentages higher and lower than 100% indicate an over- or under- identification of pixels, respectively. Though the dilation process introduced variation in total surface area coverage, most notably when the surface area coverage exceeded 100%, a comparable margin of error was still present without the dilation process, so it can be inferred that the experiment's imaging conditions were the primary reason for this inaccuracy. Images with varying locations and intensities of glare, exposed metal hardware, or shadow between shards contain colors that do not neatly fit RGB criteria, and may affect the resulting total surface area coverage. An example of over- and under-identification of pixels is shown in Figure 4 and Table 1, which show a range of red, blue, and green shard pixel coverages identified by the automated processing. Notably, the shard coverage percentages varied depending on shard organization and color arrangement. The changes in each color's coverage indicate movement within the experimental tube and changes in relative surface area coverage over time. Although the experiment took place in a passive microgravity environment for the entire duration, the shard contents occasionally left a gap near the "top"

iss050e021925		iss051e002423		iss049e014658	
Red	10.17 %	Red	53.32 %	Red	69.75 %
Green	57.05 %	Green	32.37 %	Green	13.30 %
Blue	19.98%	Blue	14.30 %	Blue	28.52 %
Total	87.20 %	Total	100.00 %	Total	111.57 %

Table 1. Identified RGB and total surface area coverage percentages for the images shown in Figure 4, highlighting the full range of results achieved through this automated procedure.

iss050e021925 (top left)	**iss051e002423 (top right)**	**iss049e014658 (bottom left)**
Dominated by blue and green	Relatively even split between colors	Dominated by red
Shards loosely packed	Shards fairly compact	Shards very loose
Visible shards are large	Visible shards are large and small	Visible shards are small
Minimal empty space at top	Relatively large empty space at top	Minimal empty space at top
Colors in clusters	Colors in clusters	Colors distributed across tube

Figure 4. Examples of images that resulted in a range of identified surface area coverage percentages (see Table 1), with descriptions of visual differences in the images that may contribute to the range of colored pixel identification and the corresponding coverage numbers.

THE PEGASUS REVIEW:
UNIVERSITY OF CENTRAL FLORIDA
UNDERGRADUATE RESEARCH JOURNAL

URJ

Vol. 15.1 : 21-31

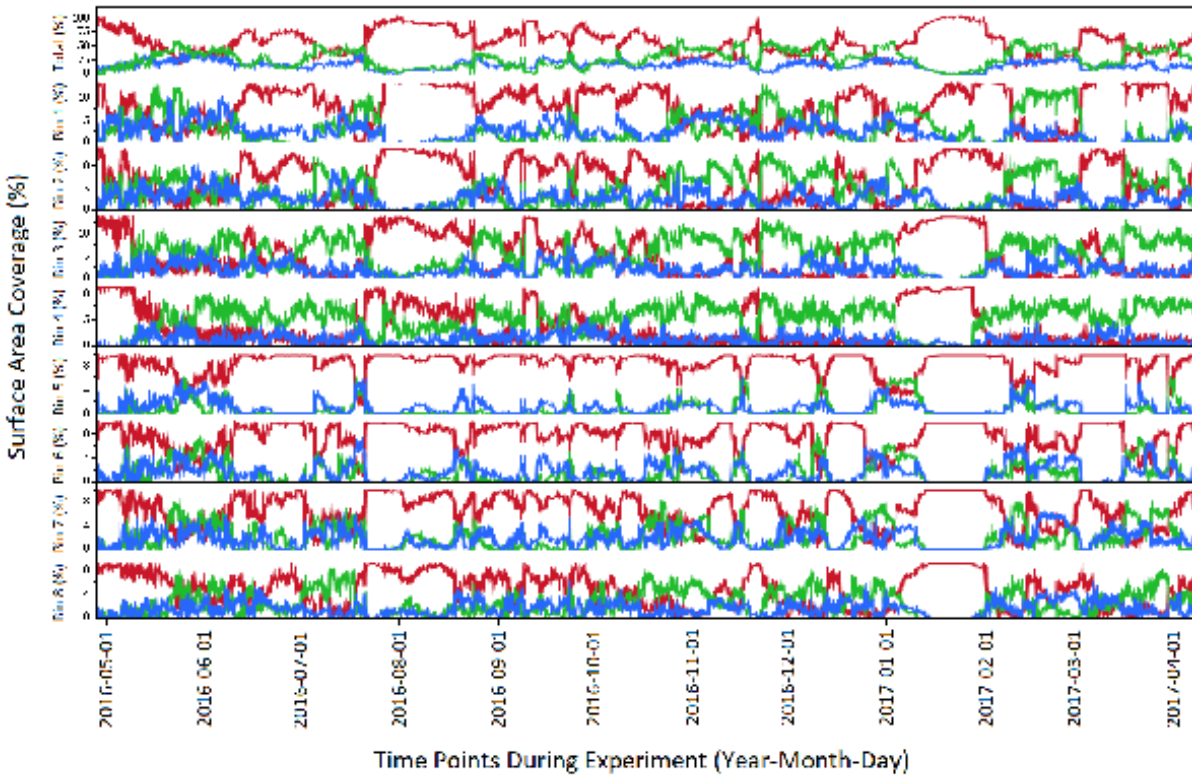

Figure 5. Red, green, and blue surface area coverage percentages identified by automated processing for the whole tube (top row) and for each bin's contribution to the total image surface area coverage across the entire lifetime of the experiment. Note that the difference in the maximum values of the y-axis between Bins 1-4 and Bin 5-8 is due to the size differences in bins, not a systematic decrease in particles in the lower portion of the tube.

portion of the tube but no other region. This may suggest a currently unknown, yet notable force aboard the ISS, causing the shards to remain lower in the tube or aggregate.

The automated procedure was able to effectively highlight where shards of a particular color set were located across the 8 image bins throughout the experiment time, as shown in Figure 5. Each color's surface area coverage was retrieved and plotted as a function of the total surface area over time. Due to the metal bar's location when spliced out of the original images, Bins 1-4 are larger and result in a larger total surface area percentage than Bins 5-8. Movement patterns of red, green, and blue shards were generally consistent across Bins 1-4 and again through Bins 5-8. Across this dataset, there were notable prolonged periods of inactivity across all bins at the beginning, from roughly mid-July to mid-August, and again throughout January. There were also shorter periods of time that imply major shard activity, indicated by the rapid shifts in surface area coverage by each shard color, which occurred around the start of June, throughout the first half of July, in the second half of October, near the beginning of January, in mid-February and again in mid-March. Interestingly, there were also movements generally consistent across left and right portions of the experiment tube: Bins 3, 4, 7, and 8 showed activity in late June, while Bins 1, 2, 5, and 6 were less active.

While the attempt to manually track individual shards over time proved to be difficult to verify due to the variable timing of the imaging sequences, we were able to manually assess relative RGB coverage for subsets of images shown in Figure 6. We found that these manual assessments showed the same trends in the RGB percent coverages generated by automatic image-processing; however, automated processing identified more details of the movements over time.

THE PEGASUS REVIEW:
UNIVERSITY OF CENTRAL FLORIDA
UNDERGRADUATE RESEARCH JOURNAL

URJ

Vol. 15.1 : 21-31

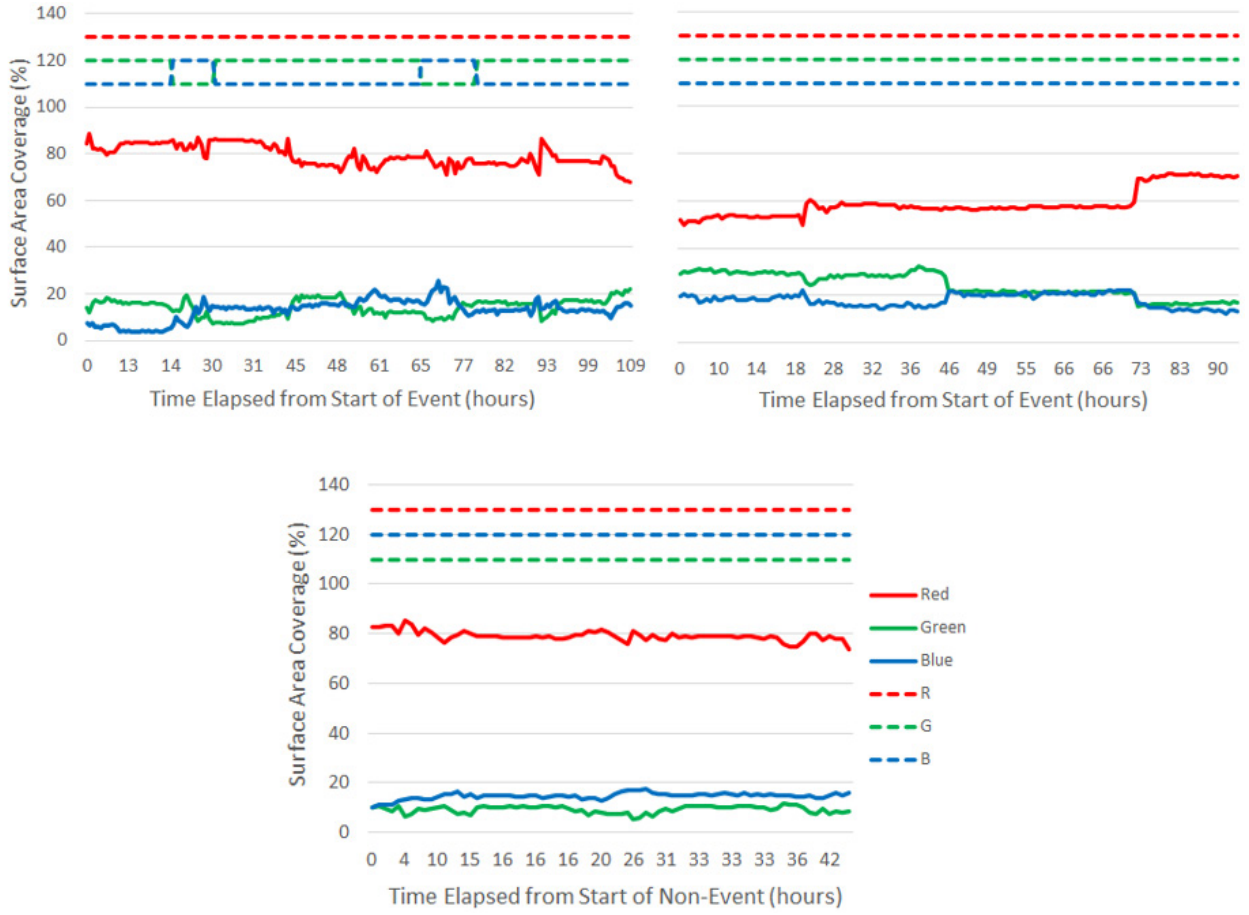

Figure 6. Automated versus manual assessments of relative red, green, and blue surface area coverages for Event 1 (top left), Event 2 (top right), and Non-Event 2 (bottom). Solid lines Red, Green, and Blue are calculations performed via automated analysis, while dotted lines R, G, and B represent the relative presence of shards as defined manually (arbitrarily set above 100%, but indicating low (110), medium (120), and high (130) coverage).

Additional data from the manual analysis tracked movement patterns, which cannot be inferred from the automated analysis. When characterizing shard movement behavior patterns, Wiggling was the most noted behavior in image subsets taken in quick succession, while subsets obtained over much longer periods of time were better defined by Swirling and other behaviors, shown in Figure 7. Because the "Fast" segments only captured a few minutes in real-time, it is fitting that small motions were mostly observed. In the "Slow" periods, much more motion may have occurred between images, which were spaced out in time, so that it may be observed in a greater variety of patterns and behaviors.

DISCUSSION

Although the image processing was challenging due to resolution, distortion by a fish-eye lens, and areas of excessive glare and shadow, identification of the RGB pixels resulted in valuable information on shard locations across the experiment surface area over time. It is evident, despite the imperfections, that this color channel separation and identification approach was able to provide unique insights on the change in colored shard coverage throughout the duration of the experiment. Automating color identification is a much faster (and more practical) alternative to manually counting and locating shards, and it removes assumptions of whether a shape is a single shard with additional overlap or multiple shards. By focusing only on the distribution of color across the surface area, we can quickly identify

THE PEGASUS REVIEW:
UNIVERSITY OF CENTRAL FLORIDA
UNDERGRADUATE RESEARCH JOURNAL

URJ

Vol. 15.1 : 21-31

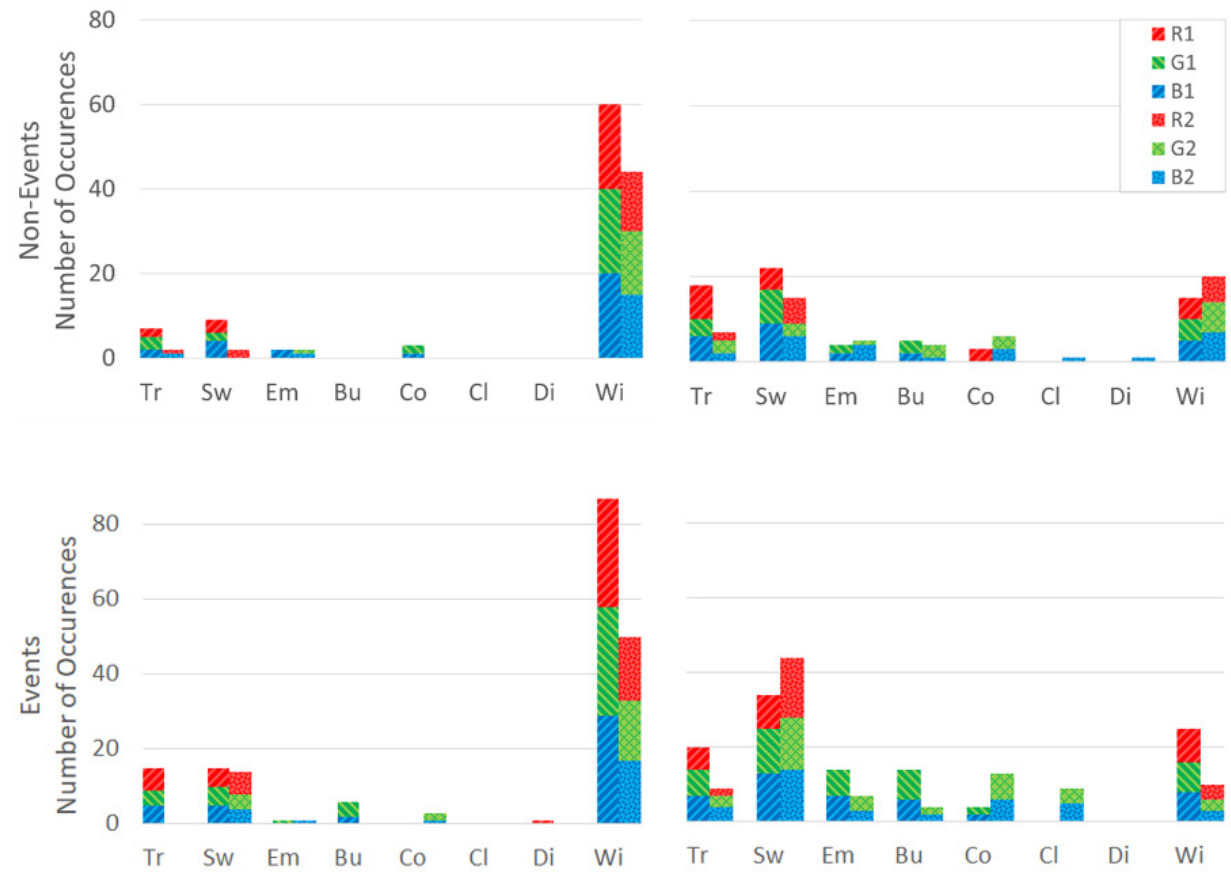

Figure 7. Manual shard movement characterizations of fast subsequence (left) and slow subsequence (right) images across all Non-Events (top row) and Events (bottom row). RGB labels followed by 1 and 2 denote datasets generated by independent data collectors, referred to as Student 1 and Student 2, respectively. Movement types include Translation (Tr), Swirling (Sw), Emerging (Em), Burying (Bu), Compaction (Co), Clustering (Cl), Dispersal (Di), and Wiggling (Wi).

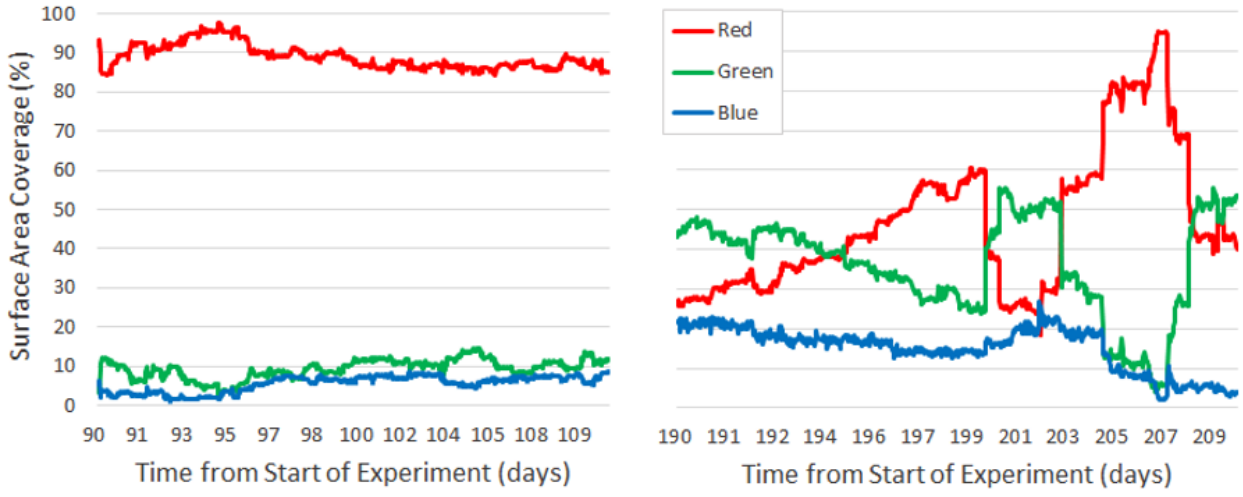

Figure 8. Examples of inactive (left) and active (right) subsets of the data.

THE PEGASUS REVIEW:
UNIVERSITY OF CENTRAL FLORIDA
UNDERGRADUATE RESEARCH JOURNAL

URJ

Vol. 15.1 : 21-31

relative shard locations and assess color dominance in each region of the experiment tube. The automated and manual assessment of RGB relative coverage were qualitatively consistent, validating the automated approach for obtaining visual insights on the Strata-1 Slot 1 data.

As previously shown in Figure 5, there were extended periods of major activity and inactivity that seemed consistent in various regions simultaneously or at different times, including within bins solely on the left and right halves, bins only near the top or bottom of the tube, or across all bins. By focusing solely on these time periods of interest, we can take a closer look at the overall shifts in total surface area coverage by red, green, and blue shards (see Figure 8). While the variation in the image-capturing sequence did not exceed 64 minutes, multiple sequences spanning days to full months may reflect physical disturbances to the experiment. The shard movements within these periods of major activity or inactivity would have been influenced by the environmental conditions aboard the ISS and constitute further exploration of the nature of those disturbances.

Initially, we manually identified Events and Non-Events due to visual cues within image sets, depending on relative activity levels. Here, these hypothesized Events and Non-Events are supported by quantitative data that indicate a rapid shift in color surface area predominance or a period of consistency.

FUTURE WORK

The existence of Events and Non-Events warrants further investigation into the accelerometer data that accompanied the Strata-1 experiment aboard the ISS. We intend to identify any significant shifts in ISS activity that align with Events suggested by our image analysis to see if these Events have specific catalysts for shard movement. The reference to the accelerometer data and ISS activity log as well as the image processing approach will form the basis for analyzing additional slots from the Strata-1 experiment.

Though the automated analysis was qualitatively similar to the manual analysis and provided additional insights, the next steps will include a statistical comparison of the two methods to confirm similar quality. While this analysis solely focused on red, green, and blue shards, we hope to adapt it to other color ranges for increased versatility. We intend to adapt this procedure to analyze a separate tube from Strata-1, a multi-sized and multi-colored spherical bead tube, which will be more challenging because the smallest beads tended to cling to the experiment tube walls, making them the most observable for a good portion of the image set. For the remaining two tubes from Strata-1 containing meteorite and meteorite simulant, these methods may need to be heavily adapted, or an entirely new procedure may need to be developed to analyze the monochrome materials effectively.

In the future, we will use insights from this processing to inform additional microgravity experiments to reduce the necessary pre-processing through improved lighting, reconfiguration of hardware, and the investigation of fish-eye camera lens alternatives. We hope to additionally utilize video processing for improved insights on individual particle movements and tracking. Follow-up experiments have included force sensors internal to the experiment for supplemental information regarding internal shard behavior, complementing the image analyses. This analysis approach will be adapted and reused to analyze experiments that shortly followed Strata-1, including the Strata-S1 (a suborbital flight experiment) and Hermes (a follow-up ISS experiment) projects.

ACKNOWLEDGEMENTS

The authors would like to acknowledge support from NASA Award #80NSSC21K0811 and #80NSSC19M0214.

THE PEGASUS REVIEW:
UNIVERSITY OF CENTRAL FLORIDA
UNDERGRADUATE RESEARCH JOURNAL

URJ

Vol. 15.1 : 21-31

REFERENCES

Britt, D. T., Cannon, K. M., Donaldson Hanna, K., Hogancamp, J., Poch, O., Beck, P., Martin, D., Escrig, J., Bonal, L., & Metzger, P. T. (2019). Simulated asteroid materials based on carbonaceous chondrite mineralogies. *Meteoritics & Planetary Science*, *54*(9), 2067–82. https://doi.org/10.1111/maps.13345

Chujo, T., Mori, O., Kawaguchi, J., Yano, H. (2018). Categorization of Brazil nut effect and its reverse under less-convective conditions for microgravity geology. *Monthly Notices of the Royal Astronomical Society*, *474*(4), *4447-59*. https://doi.org/10.1093/mnras/stx3092

Coelho, L. P. (2013). Mahotas: Open source software for scriptable computer vision. *Journal of Open Research Software*, *1*(1):e3. http://dx.doi.org/10.5334/jors.ac

Dove, A., Anderson, S., Gomer, G., Fraser, M., John, K., & Fries, M. (2018, March 19-23). *Regolith stratification and migration in an asteroid-like environment* [Conference presentation abstract]. 49th Lunar and Planetary Science Conference, The Woodlands, TX. LPI Contribution No. 2083, 2993.

Fries, M., Abell, P., Brisset, J., Britt, D., Colwell, J., Dove, A., Durda, D., Graham, L., Hartzell, C., Hrovat, K., John, K., Karrer, D., Leonard, M., Love, S., Morgan, J., Poppin, J., Rodriquez, V., Sánchez-Lana, P., Scheeres, D., & Whizin, A. (2018). The Strata-1 experiment on small body regolith segregation. *Acta Astronautica*, *142*, 87-94. https://doi.org/10.1016/j.actaastro.2017.10.025

Fries, M., Abell, P., Brisset, J., Britt, D., Colwell, J., Durda, D., Dove, A., Graham, L., Hartzell, C., John, K., & Love, S. (2016, March 21-25). *Strata-1: An International Space Station experiment into fundamental regolith processes in microgravity* [Conference presentation abstract]. 47th Lunar and Planetary Science Conference, The Woodlands, TX. LPI Contribution No. 1903, 2799.

Güttier, C., Von Borste, I., Schräpler, R., & Blum, J. (2013). Granular convection and the Brazil nut effect in reduced gravity. Physical Review E: Statistical, *Nonlinear & Soft Matter Physics*, *87*(4–B), 1-4. https://doi.org/10.1103/PhysRevE.87.044201

Klimek, R., Wright, T. (2006). Spotlight-8 Image Analysis Software, NASA/TM-2006-214084. Glenn Research Center, Cleveland OH.

Matsumura, S., Richardson, D. C., Michel, P., Schwartz, S. R., & Ballouz, R. (2014). The Brazil nut effect and its application to asteroids. *Monthly Notices of the Royal Astronomical Society*, *443*(4), 3368-80. https://doi.org/10.1093/mnras/stu1388

Maurel, C., Ballouz, R.L., Richardson, D.C., Michel, P., Schwartz, S.R. (2017). Numerical simulations of oscillation-driven regolith motion: Brazil-nut effect. *Monthly Notices of the Royal Astronomical Society*, *464*(3), 2866–81. https://doi.org/10.1093/mnras/stw2641

Miyamoto, H.,Yano, H., Scheeres D., Abe S., Barnouin-Jha O., Cheng, A., Demura, H., Gaskell, R., Hirata, N., Ishiguro, M., Michikami, T., Nakamura, A., Nakamura, R., Saito, J., & Sasaki, S. (2007). Regolith migration and sorting on asteroid Itokawa. *Science*, *316*(5827), 1011-14. https://doi.org/10.1126/science.1134390

NASA. (2012). In-Situ Resource Utilization Mission. In Nasa Facts (FS-2012-07-026-JSC). essay, Lyndon B. Johnson Space Center.

Rosato, A., Strandburg, K. J., Prinz, F., & Swendsen, R. H. (1987). Why the Brazil nuts are on top: Size segregation of particulate matter by shaking. *Physical Review Letters*, *58*(10), 1038-40. https://doi.org/10.1103/PhysRevLett.58.1038

Zhao, Z., Wang, S., Li, D., Wang, H., Wang, Y., & Zhao, J. (2019). Development of an anchoring system for the soft asteroid landing exploration. *International Journal of Aerospace Engineering*, 2019, 1-13. https://doi.org/10.1155/2019/1257038